ACS Photonics

Article

pubs.acs.org/journal/apchd5

Exciton-Polaritons with Size-Tunable Coupling Strengths in Self-Assembled Organic Microresonators

Xuedong Wang,[†,‡] Qing Liao,*[,§] Zhenzhen Xu,[†,‡] Yishi Wu,[†] Lang Wei,[†] Xiaomei Lu,[§] and Hongbing Fu*[,†,§]

[†]Beijing National Laboratory for Molecular Sciences (BNLMS), Institute of Chemistry, Chinese Academy of Sciences, Beijing, 100190, China

[‡]University of Chinese Academy of Sciences, Beijing, 100039, China

[§]Department of Chemistry, Capital Normal University, Beijing, 100048, China

Supporting Information

ABSTRACT: Self-assembled nano/microcrystals of organic semiconductors with regular faces can serve as optical microresonators, which hold a promise for studying the light confinement and the light-matter interaction. Here, single crystalline microribbons of 1,4-bis(2-(4-(*N*,*N*-di(*p*-tolyl)-amino)phenyl)-vinylbenzene (DPAVB) are synthesized with well-controlled sizes by a facile solution-exchange method. We find that individual microribbon can work as Fabry-Pérot (FP) resonator along its width (w), in which strong coupling of optical modes with excitons results in the formation of exciton polaritons (EPs). The dispersion relation of $E \sim k_z$ of EPs is constructed by extracting the energies (E) of FP resonances at integer multiples of π/w in the wavevector (k_z) space. By simulating the significantly curved dispersion of EPs with a two coupled harmonic oscillator model, a coupling strength between 0.48 and 1.09 eV are obtained. Two coupling regimes are classified: in regime I, the coupling strength is constant at 0.48 eV for microribbons with the cavity length of $w \geq 2.00$ μm; in regime II, the coupling strength increases dramatically from 0.48 to about 1 eV with decreasing the resonator length from $w = 2.00$ to 0.83 μm. More significantly, our results suggest that the exciton-photon coupling strength could be modulated by varying the size of microribbon cavities, providing an effective method for engineering the light−matter interaction in organic single crystalline microstructures.

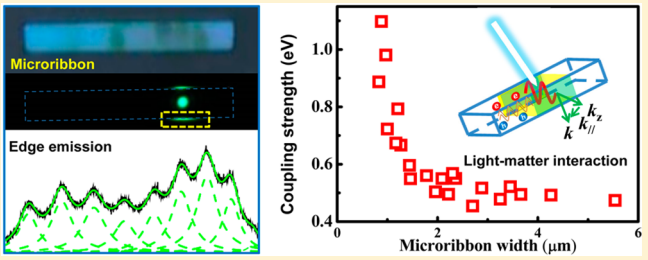

KEYWORDS: *light−matter interaction, organic semiconductor, self-assembly, size-tunable*

Since the first observation of exciton-polaritons (EPs) in a semiconductor quantum microcavity,[1] there has been considerable research interest in their quantum statistical behaviors. The part-light and part-matter feature of EPs enables the observation of Bose−Einstein condensation (BEC) in the solid-state,[2] low-threshold polariton lasing[3−5] and is also beneficial for terahertz polariton emitter,[6] and slow-light applications.[7,8] To date, most studies of EPs have been realized in planar microcavities made by a pair of distributed Bragg reflectors (DBRs),[3,9−15] in which the active media is placed at the antinodes of the intracavity light field to maximize the interaction between the excitons and the cavity modes. Recently, it was shown that strong coupling can also occur in optical waveguide configurations,[16−18] which strongly confine photons. In this case, optical modes couple with excitons of the active media, leading to the formation of exciton-polaritons (EPs). Compared with localized EPs in planar microcavities, EPs in microribbon permit the propagation of EPs and are more suitable for integration into miniaturized optical devices.

The exciton-photon coupling leads to the lower polariton branch (LPB) and the upper polariton branch (UPB) with an energy separation called Rabi splitting ($2V$),[3,19] which is a direct measure of the coupling strength (V) between the exciton and the light. The value of Rabi splitting is given by the equation, $V \propto (n \times f/V_m)^{1/2}$,[16,20] with n the number of exciton oscillators, f the exciton oscillator strength, and V_m the optical mode volume. As the large binding energy (~1 eV) and the large oscillator strength of Frenkel excitons in organic crystal, Rabi-splitting value up to hundreds of meV makes EPs in organic semiconductor microcavities highly stable at room temperature.[3,13,20,21] Since the pioneer work by Lidzey and co-workers, strongly coupled planar-microcavities have been demonstrated for a number of organic semiconductors, which are mainly composed either of disordered mixtures of *J*-aggregates in a host polymer matrix or of polycrystalline films.[19] Most recently, Forrest and co-workers demonstrated that crystalline microcavities are superior due to their high degree of structural order and observed room-temperature polariton

Received: December 9, 2013
Published: April 22, 2014

lasing from a microcavity composed of a melt-grown single-crystal layer of anthracene sandwiched between two DBRs.[3]

Self-assembly has provided a powerful method to prepare single-crystalline nano- and microstructures of organic semiconductors. Self-assembled nano/microcrystals with regular faces was demonstrated to be able to serve as active optical waveguide resonators,[16,17,22−24] providing a new platform for studying the optical confinement and realizing the light−matter interaction. Herein we report on size-tunable exciton-photon coupling in self-assembled organic single crystalline microribbons. The facile solution self-assembly method has the potential for easily fabricating size-controlled microribbons of 1,4-bis(2-(4-(*N*,*N*-di(*p*-tolyl)amino)phenyl)-vinylbenzene (DPAVB) by varying the sampling time.[25−27] We found that individual microribbon can work as Fabry-Pérot (FP) resonator along its width (w), in which strong coupling of optical waveguide modes with excitons results in the formation of exciton polaritons (EPs). The dispersion relation of $E \sim k_z$ of EPs is constructed by extracting the energies (E) of FP resonances at integer multiples of π/w in the wavevector (k_z) space. By simulating the significantly curved dispersion of EPs with a two coupled harmonic oscillator model, a coupling strength between 0.48 and 1.09 eV are obtained. Two coupling regimes are classified: in regime I, the coupling strength is constant at 0.48 eV for microribbons with the cavity length of $w \geq 2.00$ μm; in regime II, the coupling strength increases dramatically from 0.48 to about 1 eV with decreasing the resonator length from $w = 2.00$ to 0.83 μm. Our results suggest that the exciton-photon coupling strength could be modulated by varying the size of microribbon cavities, providing an effective method for engineering the light−matter interaction in organic microstructures.

RESULTS AND DISCUSSION

Microribbons of DPAVB were obtained by a solution-exchange method. Typically, 2 mL of ethanol, which serves as the poor solvent, was dropwise added into 0.1 mL of a stock solution (10 mM) of DPAVB dissolved in tetrahydrofuran (THF). The turbulent mixing of ethanol with DPAVB/THF solution changes the solvent surroundings, thus, initiating the nucleating and assembling processes. After 1 h (sampling time), yellow precipitates were centrifugally separated from the suspension and washed using poor solvent of ethanol. Scanning electron microscopy (SEM) image of Figure 1a depicts that as-prepared microribbons have regular shapes and optical faces. Figure 1b displays the selected area electron diffraction (SAED) pattern recorded by directing the electron beam almost perpendicular to the flat surface of corresponding microribbon (shown in the inset of Figure 1b). The X-ray diffraction (XRD) measurement of microribbons shows the first peak is located at 4.34°, which corresponds to the interplanar spacing of 20.35 Å. This spacing of 20.35 Å is similarly identical to the long axis of DPAVB molecule 26.72 Å obtained by Gaussian simulation (Figure S1, Supporting Information); therefore, the peak at 4.34° is labeled as (001). Further it is found that only a sequence of peaks corresponding to (001) crystal planes is presented in the XRD measurements. The observation of high-order diffraction peaks that is (002), (003), (004), (005), and (006) suggests that microribbons adopt a lamellar structure with the crystal (001) plane parallel to the substrate. Meanwhile, we conduct polarized photoluminescence (PL) measurements at three positions denoted by circles on one sample microribbon in Figure S2. The same polarization anisotropy indicates that the

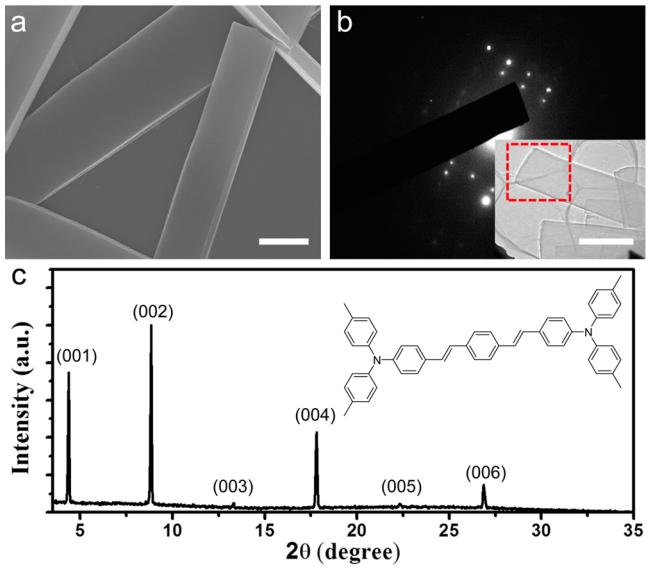

Figure 1. (a) SEM image of as-prepared DPAVB microribbons. Scale bar is 2 μm. (b) SAED pattern of one microribbon, as shown in the inset of TEM image with a scale bar of 2 μm, and the red dashed square denotes the region for SAED pattern. (c) XRD pattern of ensemble microribbons filtered on the surface of an alumina membrane. Inset: the chemical structure of DPAVB molecule.

form of molecule packing is the same within the entire domain of one microribbon. Individual microribbons were further imaged by atomic force microscopy (AFM), revealing their perfect smooth surfaces and sharp edges (Figure 2a). According to the height profiles in insets of Figure 2a, the thickness (h) of corresponding ribbons are also calculated, and Figure 2b shows the histogram of thickness distribution of microribbons by randomly measuring the AFM profiles of 10 sample microribbons on a glass substrate, and the height (h) of the DPAVB microribbons ranges from 0.20 to 0.45 μm. Based on the above measurements, these as-prepared microribbons are single crystalline microstructures with regular shapes and smooth faces.

To investigate the influence of cavity size on the light−matter coupling strength in DPAVB microribbon microresonators, controlled different sizes of DPAVB microribbons can be obtained by varying sampling time. Figure 3a−c shows optical images of microribbons with an average width (w) ranging from 1.0 to 2.5 μm, and to 5.0 μm, obtained at sampling time from 30 min to 2 h, and to 6 h, respectively. From these optical images of microribbons it is confirmed that the length L of microribbons ranges from 10 to 30 μm. The SEM images of these microribbons with different width (w) are shown in the inset of Figure 3a−c. The corresponding photoluminescence (PL) microscopy images (Figure 3d−f) of microribbons show strong green fluorescence and brighter fluorescence at the edges of microribbons, which indicate that the as-prepared individual microribbon could work as active media of fluorescence emission.

Figure 4a shows the absorption (dashed line) and fluorescence (solid line) spectra of DPAVB molecules in THF solution (black line) with a concentration of 10^{-5} M (top panel). In striking contrast to those of the monomers, the absorption and emission of DPAVB microribbons (red line) exhibit bathochromically shifted and narrow bands (bottom panel of Figure 4a). This implies that the DPAVB molecules of

dx.doi.org/10.1021/ph400160v | ACS Photonics 2014, 1, 413−420

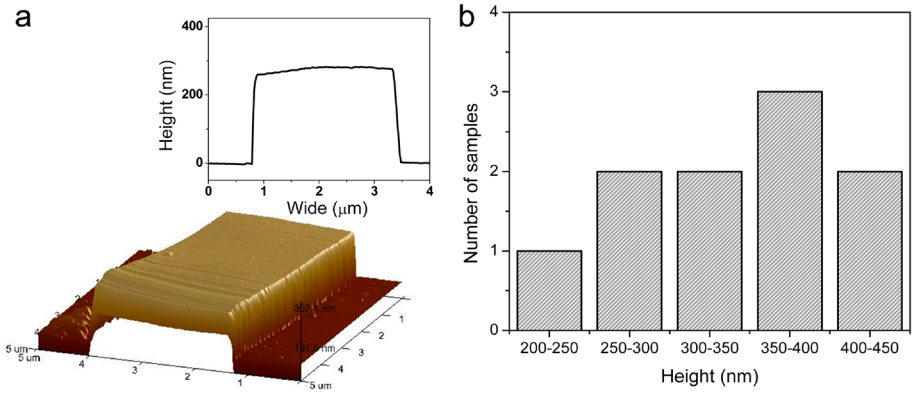

Figure 2. (a) AFM image and corresponding height profile of one sample microribbon. (b) The histogram of thickness distribution of microribbons by randomly measuring the AFM profiles of 10 samples on a glass substrate. The height (h) of the DPAVB microribbons ranges from 0.20 to 0.45 μm.

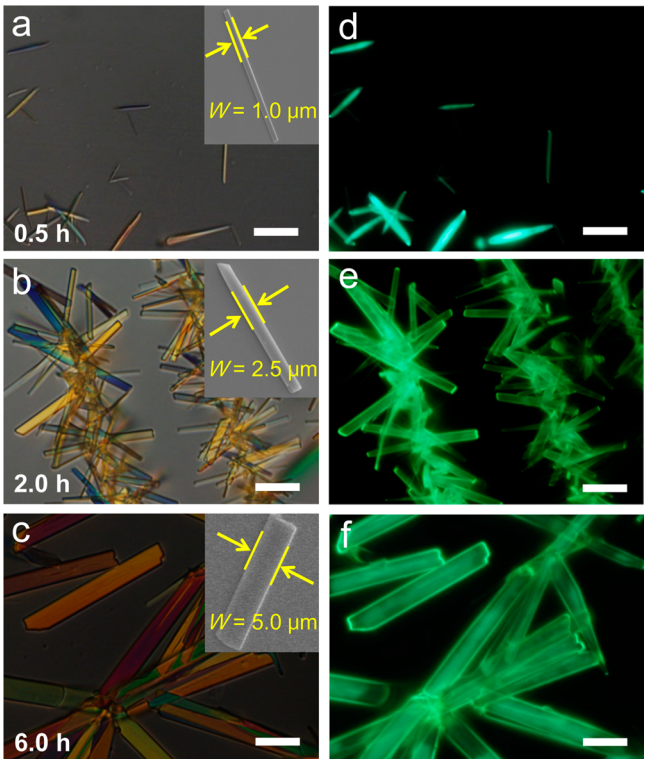

Figure 3. Bright-field optical micrograph of microribbons with tunable sizes obtained at different sampling times: (a) 30 min with w = 1.0 μm, (b) 2 h with w = 2.5 μm, and (c) 6 h with w = 5.0 μm. Inset: the SEM image of corresponding microribbons. (d–f) Corresponding fluorescence microscopy images of microribbons with different sizes excited with UV light (330–380 nm) from a mercury lamp. All the scale bars are 10 μm.

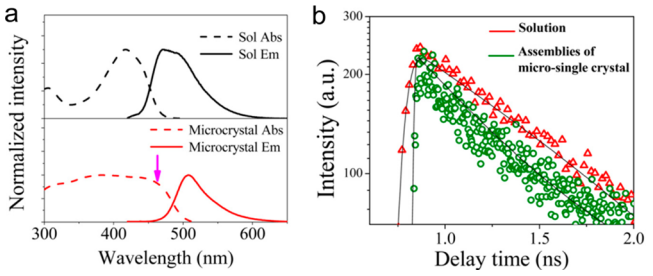

Figure 4. (a) Absorption (dashed line) and fluorescence (solid line) spectra of DPAVB molecules in THF solution (black line) with a concentration of 10^{-5} M (top panel); and absorption and fluorescence (red line) spectra of ensemble microribbons placed on a quartz plate (bottom panel). (b) Fluorescence decay profiles of DPAVB monomers in THF solution (red) and ensemble microribbons (green). The excitation wavelength is at 400 nm.

microribbons are in the formation of the J-aggregate.[28,29] The J-aggregated molecules with enhanced oscillator strength in microribbons are beneficial for strong exciton–photon interaction. To further confirm the J-aggregation of DPAVB microribbons, we investigated the PL lifetimes with a streak camera. The DPAVB solution PL at 500 nm follows single exponential decay with τ = 1.23 ± 0.01 ns and the DPAVB solution also follows single exponential decay with τ = 1.60 ± 0.03 ns (Figure 4b). The obtained PL quantum yield and lifetimes of DPAVB samples are presented in Table S1. Therefore, the radiative decay rates k of DPAVB monomers and microribbons are calculated to be $k_{monomer}$ = 0.76 ns^{-1} and $k_{microribbon}$ = 0.99 ns^{-1}, respectively, according to the equation, $k_F = \Phi/\tau$.[30] The result that $k_{solution} < k_{microcrystal}$ is also consistent with the J-aggregation model.[29] The J-aggregates of DPAVB crystalline microribbons hold a promise for the strong exciton–photon coupling and the formation of exciton–polariton in these self-assembled microribbon microcavities.

In order to investigate the influence of cavity size on the light–matter interaction in DPAVB microribbons, a homemade confocal fluorescence microscopy system is used (see more details in Figure S3). The excitation laser beam (λ = 408 nm) was focused down to a spot size around 1 μm at the body of single DPAVB microribbon (as shown in Figure 5a), and spatially resolved PL spectra were collected underneath using another 3D-movable objective coupled to an optical fiber and detected using a liquid-nitrogen cooled charge-coupled device (CCD). Figure 5b shows the optical image of one sample microribbon and Figure 5c presents the PL microscopy image of this microribbon excited with a focused 408 nm laser beam. Figure 5d shows the PL spectrum obtained at the excitation position (top panel) marked with the red circle, and the spectrum obtained at the edge position (bottom panel) is denoted by a yellow dashed square. At a closer look of these two spectra, a series of resonance peaks are observed on the PL spectrum obtained at the edge position, while the smooth profile of the PL spectrum of the DPAVB crystal is obtained at the excitation position. This resonance phenomenon indicates

dx.doi.org/10.1021/ph400160v | ACS Photonics 2014, 1, 413–420

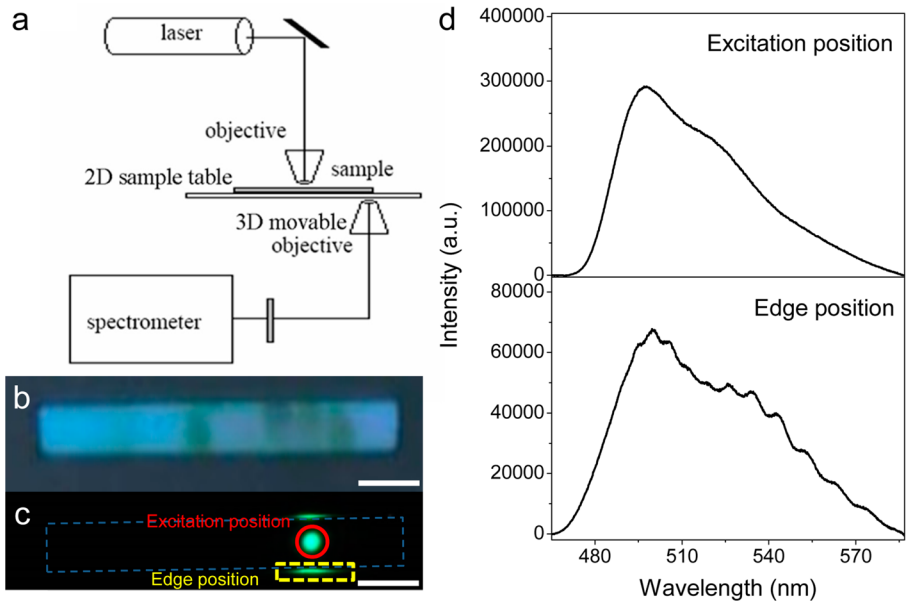

Figure 5. (a) Schematic illustration of the transmittance optical path for the spatially resolved PL measurements. (b) Optical image of one sample microribbon. Scale bar is 5 μm. (c) Fluorescence microscopy image of the same microribbon locally excited with a focused 408 nm laser beam. The excitation position is denoted with the red solid circle and the position of edge emission is marked with a yellow dashed square line. (d) The PL spectrum at the excitation position (top panel) and the PL spectrum at edge position (bottom panel).

that the standing wave modes (FP mode) are formed along the width direction of the microribbon.

The optical modulation of FP resonance in microribbons could be better analyzed by fitting the individual microribbon PL spectrum with Lorentzian line. For instance, the spacing between peaks (two adjacent peaks) is 9.45, 7.32, and 3.30 nm at 500 nm for three sample microribbons with width w of 1.89, 2.90, and 6.63 μm, respectively (Figure 6a). This presents an increasing number of FP modes with the increasing microribbon width (w), which is identical to the FP cavity length. Furthermore, the simulation of two-dimensional (2D) electric field distribution along the cross section of the microribbon (Figure S4a–c) confirms that the FP mode exists in the width direction of the microribbon. For the PL spectra of FP-type resonance, the mode spacing $\Delta\lambda_m$ is given by

$$\Delta\lambda_m = \frac{\lambda^2}{2wn_g} \quad (1)$$

where w is the width of the microribbon, λ is the light of wavelength, and n_g is the group refractive index as a function of the wavelength. A plot of $1/w$ of the microribbons versus the mode spacing $\Delta\lambda_m$ at 500 nm is shown in Figure 6b. The best-fit line (black line) is clearly linear, which confirms that the microribbon operates as FP mode resonator along the width direction rather than other dimensions of the microribbon. The group refractive index n_g corresponding to the emission regime could be calculated to profile the optical dispersion relations in active FP cavities along the width of microribbon, as plotted in Figure 6c. The group refractive index n_g value shows a trend of slowly decrease with the increasing of wavelength in the emission band, which is identical in these three microribbons with different widths. These enormously high values of n_g with slowly decrease trends indicates extremely strong exciton-photon coupling happened in these assembled microribbons and the formation of exciton-polaritons (EP) quasi-particles.[17]

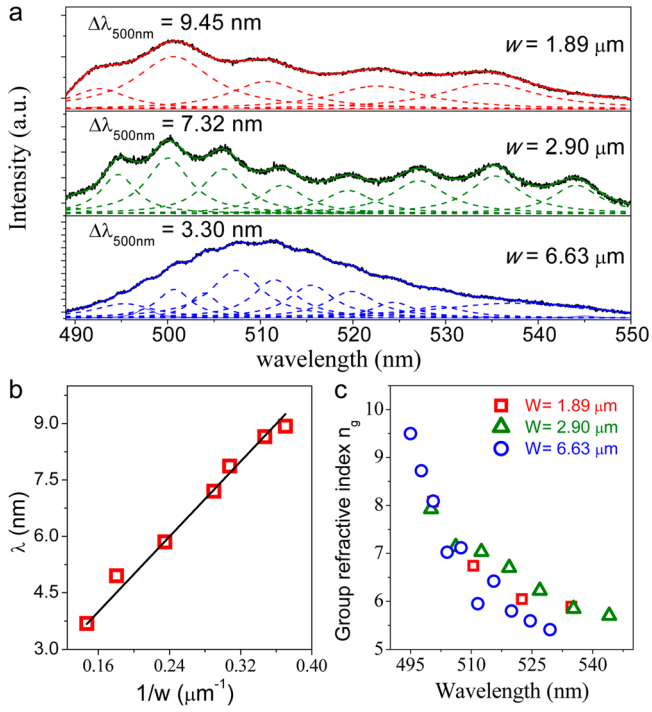

Figure 6. (a) μ-PL spectra of three microribbons with different widths w of 1.89, 2.90, and 6.63 μm, respectively. The spectra show the modulation of Fabry-Pérot (FP) mode in microribbons with different size. (b) Mode spacing at 500 nm vs $1/w$ (w: the width length) of a microribbon, showing clearly a linear relationship. (c) The plots of group refractive index n_g vs wavelength in three microribbons with different widths.

Thus, the observed series of resonance peaks on the PL spectrum could be attributed to the polariton emission.

To know the exact value of exciton–photon coupling strength for different microribbons, we use a coupled two harmonic oscillator given by

dx.doi.org/10.1021/ph400160v | ACS Photonics 2014, 1, 413–420

$$\begin{pmatrix} E_{ph} & V \\ V & E_{ex0-0} \end{pmatrix}\begin{pmatrix} \alpha \\ \beta \end{pmatrix} = E\begin{pmatrix} \alpha \\ \beta \end{pmatrix} \quad (2)$$

interaction potentials (V) and uncoupled exciton energies (E_{ex} = 2.86 eV for 0−0 transition, denoted by a pink arrow in the absorption spectrum of assembled microribbons), the energy of polariton state (E), and mixing coefficients (photonic $|\alpha|^2$ and excitonic $|\beta|^2$) of the corresponding polariton state. E_{ph} is the cavity photon given by

$$E_{ph} = \frac{\hbar ck}{\sqrt{\varepsilon_0}} = \frac{\hbar c\sqrt{k_{||}^2 + k_z^2}}{\sqrt{\varepsilon_0}} \quad (3)$$

the reduced Planck constant ($\hbar$), speed of light in vacuum (c), the wavevector of polariton (k), and the relative permittivity (ε_0 = 3.24 of our organic materials). $k_{||}$ is the wave vector perpendicular to the path of FP mode along the width of microribbons and k_z is the wave vector parallel to the path of light. Since there is no spatial distribution of component of $k_{||}$ in our system, then the k is equal to k_z. Figure 7a−c shows three example PL spectra for microribbons with different widths ranging from 4.35 to 1.78 μm, and to 0.97 μm, respectively. These PL spectra could be fitted by Lorentzian line shapes to better determine the resonance energies. Spatial dispersion is omitted since in our investigated energy range the upper polarion branch (UPB) is severely damped and only modes on the lower polariton branch (LPB) propagate within the microribbon. In Figure 7d−f, we could reconstruct the corresponding energy ∼ wavevector ($E \sim k_z$) dispersion of propagating modes by placing the interference peaks at integer multiples of π/w in the space of k_z.[31] The obtained $E \sim k_z$ dispersion of the propagating modes exhibits significant curvature. We simulated this polariton dispersion using eq 2, with settled E_{ex0-0}. The value of E_{ex0-0} = 2.86 eV is related to the 0−0 transition, which corresponds to the peak (pink arrow denoted) in the absorption spectrum (red dashed line in Figure 3a) of assembled DPAVB microribbons. And the option of E_{ex0-0} = 2.86 eV is based on the fitting results of calculation (see more detailed information in Table S2).

From the simulation, we can get the coupling strength V ranging from 0.48 eV (Figure 7d), to 0.62 eV (Figure 7e), and to 0.98 eV (Figure 7f) for the corresponding example microribbon with widths w ranging from 4.35 μm (Figure 7a), to 1.78 μm (Figure 7b), and to 0.97 μm (Figure 7c), respectively. These high coupling strength V values confirm that extremely strong exciton−photon coupling exists in these microribbons, and the formation of exciton−polariton quasiparticle at room temperature. Also, from these three example microribbons, we can get the conclusion that different coupling strengths are corresponding to the cavities with different sizes. Through the coupled two harmonic oscillator model, we could get the mixing coefficients (photonic $|\alpha|^2$ and excitonic $|\beta|^2$; Figure 7d−f) of corresponding polariton state, which demonstrates the part-light and part-matter nature of exciton−polaritons in DPAVB microribbons.[32]

In order to know the correlation between exciton−photon coupling strength V and the size of microribbons, 23 microribbons with different width (w) were studied (Figure 8a). According to the value of coupling strength V, the corresponding width w of microribbons could be classified into two regimes: width w below 2.00 μm (regime I) and above 2.00 μm (regime II). We define w = 2.00 μm as the critical point to

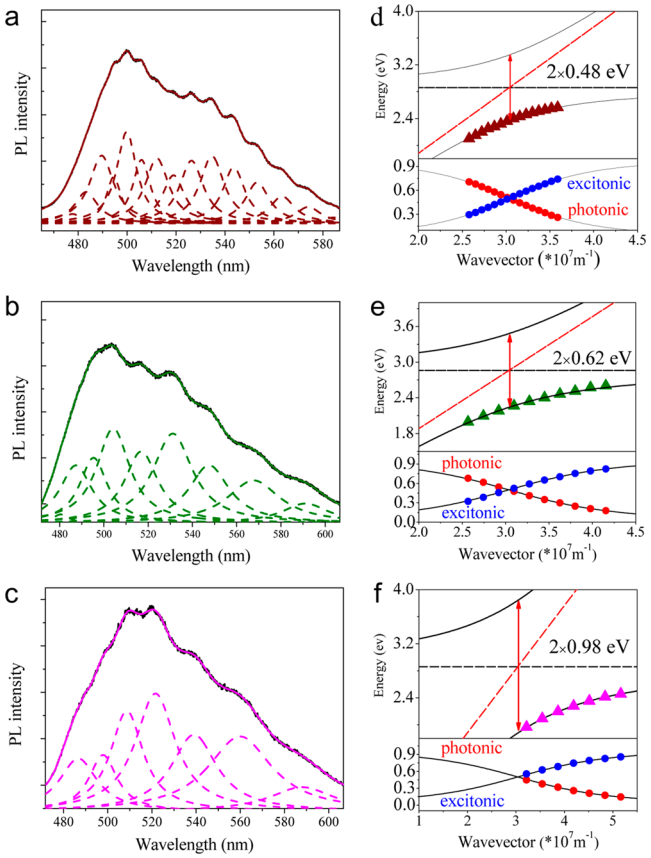

Figure 7. Photoluminescence spectra at the edge of the microribbon and size-dependent light−matter coupling strength. (a−c) PL spectra of emission collected at the guided ends (nonexcited location) of microribbons with width w of 4.35, 1.78, and 0.97 μm, respectively. (d−f) Energy-wavevector dispersion in the z-direction (along the direction of microribbon width) for the three corresponding microribbons. Top panel: The triangle data points indicate the Fabry-Pérot peaks, which have been placed in wavevector space at integer values of π/w_z with w_z being the microribbon width. The solid lines show the results of numerical calculations for the fundamental mode. Bottom panel: The red and blue circular points represent the photonic component coefficients and excitonic component coefficients of the corresponding polariton state, respectively.

depict the size-tunable coupling strength. In regime II, the coupling strength V is mainly constant at 0.48 eV, while in regime I, there is a trend that the coupling strength V increases dramatically with the decreasing width w, especially around the width 1 μm. From the introduction part, the coupling strength V is expressed as

$$V \propto \sqrt{n \times f/V_m} \quad (4)$$

where n is the number of exciton oscillators, f corresponds to the exciton oscillator strength, and V_m is the optical mode volume.

As for the case of organic DPAVB microribbons, the FP-mode cavity is formed along the width direction. And Figure 5c shows that the laser spot size was focused down to a spot size around 1 μm at the body of single DPAVB microribbon. Thus, the light-matter interaction region is not corresponding to the entire microribbon. And the light−matter interaction region is marked with the red rectangular dashed line, as shown in Figure S6a. Furthermore, Figure S6b depicts the schematic demonstration for the 3D light−matter interaction region marked with

dx.doi.org/10.1021/ph400160v | ACS Photonics 2014, 1, 413−420

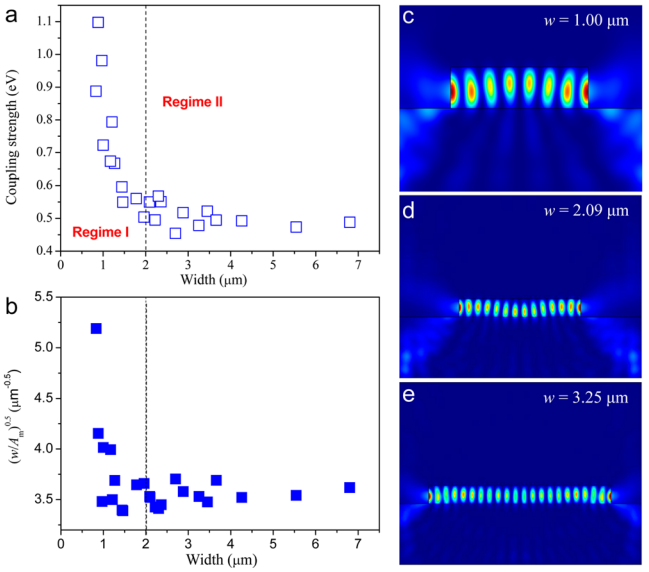

Figure 8. (a) Exciton−photon coupling strength V (blue hollow square) for 23 microribbons with widths ranging from 0.83 to 6.80 μm. (b) Calculated $(w/A_m)^{1/2}$ (blue filled square) for microribbons with a height of 0.30 μm as a function of microribbon width (w). (c−e) Plots of the electric energy density time average (J/m^3, λ = 500 nm, n = 1.80) of microribbon widths (w) of (c) 1.00, (d) 2.09, and (e) 3.25 μm. Red corresponds to the highest field density and blue is the lowest field density.

the red background. The length of this light−matter interaction region is l_{eff}, which depends on the size of the excitation laser spot (~1 μm), as shown in Figure S6a. Therefore, the l_{eff} is approximately equal to 1 μm for every microribbon microresonator.

Based on eq 4, the coupling strength V depends on the following three parameters: the number of exciton oscillators n, the exciton oscillator strength f, and the optical mode volume V_m. First of all, the number of exciton oscillators n is equal to the number of DPAVB molecules within the light−matter interaction region. As the microribbons are single crystalline, the number of exciton oscillators or DPAVB molecules within this region could be expressed by

$$n = \frac{N_a \rho V}{M} = \frac{\rho N_a l_{eff} h w}{M} \quad (5)$$

where N_a is Avogadro's constant ($N_a = 6.022 \times 10^{23}$), ρ is the density of the DPAVB crystal, M is molar mass of DPAVB (M = 672.9 g/mol), l_{eff} is the length of light−matter region (l_{eff} = 1 μm), h is the height of light−matter region (h = 0.30 μm), and w is the width of light−matter region (microribbon). In DPAVB microribbon, the density ρ, molar mass of DPAVB M, and the length of light−matter region l_{eff} are all constant values for every microribbons. Meanwhile the parameter h is fixed at 0.30 μm for microribbons. And thus the w is the only variable parameter in eq 5. Therefore, the number n of exciton oscillators is proportional to the value of width w of the microribbon.

As for the exciton oscillator strength f, it is a constant value due to the localized nature of Frenkel exciton in organic DPAVB single crystalline microribbon.[33,34] The third parameter is the optical mode volume V_m, which is based on the light−matter region in Figure S6b. As it demonstrates, the FP-mode cavity is formed along the width direction of microribbon and the electric field distribution is not confined in the length direction. And the length (L = 10−30 μm) of microribbons is far larger than the l_{eff} (l_{eff} = 1 μm). Therefore, the optical mode volume V_m could be approximately expressed as $V_m \approx A_m \times l_{eff}$, with A_m representing the mode area corresponding to the cross sectional domain marked with the red dashed region in Figure S6b. Therefore, the coupling strength V could be given by

$$V \propto \sqrt{n \times f / V_m} = \sqrt{n \times f / (A_m \times l_{eff})} = \sqrt{f / l_{eff}} \times \sqrt{w / A_m} \quad (6)$$

Based on these above analyses, the value of $(f/l_{eff})^{1/2}$ stays constant for every microribbons, and thus the coupling strength V depends on the value of $(w/A_m)^{1/2}$. The mode area A_m could be calculated according to its definition (see more details in Figure S5), and $(w/A_m)^{1/2}$ at a fixed microribbon height (h) of 0.30 μm is shown as a function of microribbon width (w) in Figure 8b. It is found that the obtained $(w/A_m)^{1/2}$ varies very little with the increasing width w ($w \geq$ 2.00 μm). However, the value of $(w/A_m)^{1/2}$ increases also dramatically with decreasing microribbon width from w = 2.00 to 0.83 μm. More significantly, from these simulation results, we find the change trend of $(w/A_m)^{1/2}$ (blue filled square in Figure 8b) is consistent with the size-tunable coupling strength V (blue hollow square in Figure 8a). Thus, w = 2.00 μm is defined as a critical point. Below this critical point, the size (w) of the microribbon could effectively modulate the coupling strength V; and when $w \geq$ 2.00 μm, the coupling strength V has little dependence on width w. Therefore, in the case of organic DPAVB microribbons, the variation of $(w/A_m)^{1/2}$ can explains for the size-tunable coupling strength V.

Figure 8c−e shows the plots of the electric energy density time average (J/m^3) of microribbon with width (w) of (c) 1.00, (d) 2.09, and (e) 3.25 μm, which confirms that this increase in $(w/A_m)^{1/2}$ for width w ranging from 2.00 to 0.83 μm is caused by the poorer electric-field confinement for the microribbon with smaller width w. Meanwhile, according to the mixing components of excitonic and photonic in three example microribbons (Figure 7d−f), higher fraction of exciton components and lower fraction of photon components are for the same polariton state in the microribbon with smaller size. It is consistent with the conclusion that the poorer photon confinement in the smaller size of microstructures.[35] Herein the size of these self-assembled optical resonators can modulate the coupling strength between photon and exciton.

CONCLUSION

We have fabricated size-controlled crystalline organic microribbons using the facile solution-exchange method. Resonance phenomena are observed in the PL emission of individual microribbon. This demonstrates that the microribbons can work as FP mode optical resonator along the width of the microribbon. The group refractive index value n_g in our system is as high as 9 due to the efficient strong coupling between photon and exciton. By simulating the polariton dispersion using a coupled two harmonic oscillator to our system, we can get the value of exciton-photon coupling strength V. The obtained high coupling strength V (0.48 ~ 1.09 eV) implies that the strong exciton−photon coupling and the effective formation of EPs at room temperature. Noteworthy in the process of studying different microribbons, it is confirmed that

dx.doi.org/10.1021/ph400160v | ACS Photonics 2014, 1, 413−420

we can modulate exciton−photon coupling strength by varying the size of microribbon. This approach to size-tunable exciton−photon coupling strength in organic crystalline DPAVB microribbons may lead to a new series of novel exciton−polariton photonic devices.

■ ASSOCIATED CONTENT

Supporting Information

Experimental details, optimized geometry of DPAVB molecule, polarized PL measurements, photophysical parameters of DPAVB sample, schematic illustration of the near-field scanning optical microscopy, simulated 2D normalized electric field distribution, simulation of polariton dispersion, the calculated mode area A_m, and the schematic demonstration for effective light−matter region. This material is available free of charge via the Internet at http://pubs.acs.org.

■ AUTHOR INFORMATION

Corresponding Authors

*E-mail: liaoqing@cnu.edu.cn.

*E-mail: hongbing.fu@iccas.ac.cn.

Notes

The authors declare no competing financial interest.

■ ACKNOWLEDGMENTS

Thanks Dr ChangLing Zou, Xiao Xiong for help in the simulation of electric field distribution. This work was supported by the National Natural Science Foundation of China (Nos. 21073200, 21273251, 91333111, 20925309, 21190034, 21221002), Beijing Municipal Science and Technology Commission (No. Z131103002813097), the National Basic Research Program of China (973) 2011CB808402, 2013CB933500, and the Chinese Academy of Sciences.

■ REFERENCES

(1) Weisbuch, C.; Nishioka, M.; Ishikawa, A.; Arakawa, Y. Observation of the coupled exciton-photon mode splitting in a semiconductor quantum microcavity. *Phys. Rev. Lett.* **1992**, *69*, 3314−3317.

(2) Kasprzak, J.; Richard, M.; Kundermann, S.; Baas, A.; Jeambrun, P.; Keeling, J. M.; Marchetti, F. M.; Szymanska, M. H.; Andre, R.; Staehli, J. L.; Savona, V.; Littlewood, P. B.; Deveaud, B.; Dang le, S. Bose−Einstein condensation of exciton polaritons. *Nature* **2006**, *443*, 409−414.

(3) Kéna-Cohen, S.; Forrest, S. R. Room-temperature polariton lasing in an organic single crystal microcavity. *Nat. Photonics* **2010**, *4*, 371−375.

(4) Yamamoto, A.; Ram, R. J.; Pau, S.; Yamamoto, Y. Nonequilibrium condensates and lasers without inversion: Exciton-polariton lasers. *Phys. Rev. A* **1996**, *53*, 4250−4253.

(5) Deng, H.; Weihs, G.; Snoke, D.; Bloch, J.; Yamamoto, Y. Polariton lasing vs. photon lasing in a semiconductor microcavity. *Proc. Natl. Acad. Sci. U.S.A.* **2003**, *100*, 15318−15323.

(6) Geiser, M.; Scalari, G.; Castellano, F.; Beck, M.; Faist, J. Room temperature terahertz polariton emitter. *Appl. Phys. Lett.* **2012**, *101*, 141118−141121.

(7) van Vugt, L. K.; Zhang, B.; Piccione, B.; Spector, A. A.; Agarwal, R. Size-dependent waveguide dispersion in nanowire optical cavities: slowed light and dispersionless guiding. *Nano Lett.* **2009**, *9*, 1684−1688.

(8) Gu, B.; Kwong, N. H.; Binder, R.; Smirl, A. L. Slow and fast light associated with polariton interference. *Phys. Rev. B* **2010**, *82*, 035313−035322.

(9) Christopoulos, S.; von Högersthal, G.; Grundy, A.; Lagoudakis, P.; Kavokin, A.; Baumberg, J.; Christmann, G.; Butté, R.; Feltin, E.; Carlin, J. F.; Grandjean, N. Room-temperature polariton lasing in semiconductor microcavities. *Phys. Rev. Lett.* **2007**, *98*, 126405.

(10) Huang, R.; Tassone, F.; Yamamoto, Y. Experimental evidence of stimulated scattering of excitons into microcavity polaritons. *Phys. Rev. B* **2000**, *61*, R7857.

(11) Das, A.; Heo, J.; Jankowski, M.; Guo, W.; Zhang, L.; Deng, H.; Bhattacharya1, P. Room temperature ultralow threshold GaN nanowire polariton laser. *Phys. Rev. Lett.* **2011**, *107*, 066405.

(12) Christmann, G.; Butté, R. l.; Feltin, E.; Carlin, J.-F. o.; Grandjean, N. Room temperature polariton lasing in a GaN/AlGaN multiple quantum well microcavity. *Appl. Phys. Lett.* **2008**, *93*, 051102.

(13) Lidzey, D. G.; Bradley, D. D. C.; Skolnick, M. S.; Virgili, T.; Walker, S.; Whittaker, D. M. Strong exciton-photon coupling in an organic semiconductor microcavity. *Nature* **1998**, *395*, 53−55.

(14) Lidzey, D. G.; Bradley, D. D. C.; Virgili, T.; Armitage, A.; Skolnick, M. S. Room temperature polariton emission from strongly coupled organic semiconductor microcavities. *Phys. Rev. Lett.* **1999**, *82*, 3316.

(15) Giebink, N. C.; Wiederrecht, G. P.; Wasielewski, M. R. Strong exciton-photon coupling with colloidal quantum dots in a high-Q bilayer microcavity. *Appl. Phys. Lett.* **2011**, *98*, 081103.

(16) van Vugt, L. K.; Piccione, B.; Cho, C. H.; Nukala, P.; Agarwal, R. One-dimensional polaritons with size-tunable and enhanced coupling strengths in semiconductor nanowires. *Proc. Natl. Acad. Sci. U.S.A.* **2011**, *108*, 10050−10055.

(17) Takazawa, K.; Inoue, J.-i.; Mitsuishi, K.; Takamasu, T. Fraction of a millimeter propagation of exciton polaritons in photoexcited nanofibers of organic dye. *Phys. Rev. Lett.* **2010**, *105*, 067401.

(18) Ellenbogen, T.; Crozier, K. B. Exciton-polariton emission from organic semiconductor optical waveguides. *Phys. Rev. B* **2011**, *84*, 161304−161307.

(19) Lidzey, D. G.; Bradley, D. D. C.; Armitage, A.; Walker, S.; Skolnick, M. C. Photon-mediated hybridization of frenkel excitons in organic semiconductor microcavities. *Science* **2000**, *288*, 1620−1623.

(20) Andreani, L. C.; Panzarini, G.; Gérard, J.-M. Strong-coupling regime for quantum boxes in pillar microcavities: Theory. *Phys. Rev. B* **1999**, *60*, 13276.

(21) Holmes, R. J.; Forrest, S. R. Strong exciton-photon coupling in organic materials. *Org. Electron.* **2007**, *8*, 77−93.

(22) Xu, Z.; Liao, Q.; Shi, Q.; Zhang, H.; Yao, J.; Fu, H. Low-threshold nanolasers based on slab-nanocrystals of H-aggregated organic semiconductors. *Adv. Mater.* **2012**, *24*, OP216−220.

(23) Zhang, C.; Zou, C. L.; Yan, Y.; Hao, R.; Sun, F. W.; Han, Z. F.; Zhao, Y. S.; Yao, J. Two-photon pumped lasing in single-crystal organic nanowire exciton polariton resonators. *J. Am. Chem. Soc.* **2011**, *133*, 7276−7279.

(24) van Vugt, L. K.; Rühle, S.; Vanmaekelbergh, D. Phase-correlated nondirectional laser emission from the end facets of a ZnO nanowire. *Nano Lett.* **2006**, *6*, 2707−2711.

(25) Zhao, Y. S.; Fu, H. B.; Peng, A. D.; Ma, Y.; Liao, Q.; Yao, J. N. Construction and optoelectronic properties of organic one-dimensional nanostructures. *Acc. Chem. Res.* **2010**, *43*, 409−418.

(26) Lei, Y. L.; Liao, Q.; Fu, H. B.; Yao, J. N. Phase- and shape-controlled synthesis of single crystalline perylene nanosheets and its optical properties. *J. Phys. Chem. C* **2009**, *113*, 10038−10043.

(27) Kang, L.; Fu, H.; Cao, X.; Shi, Q.; Yao, J. Controlled morphogenesis of organic polyhedral nanocrystals from cubes, cubooctahedrons, to octahedrons by manipulating the growth kinetics. *J. Am. Chem. Soc.* **2011**, *133*, 1895−1901.

(28) Spano, F. C. The spectral signatures of frenkel polarons in H- and J-aggregates. *Acc. Chem. Res.* **2009**, *43*, 429−439.

(29) Wurthner, F.; Kaiser, T. E.; Saha-M?ller, C. R. J-Aggregates: from serendipitous discovery to supramolecular engineering of functional dye materials. *Angew. Chem., Int. Ed.* **2011**, *50*, 3376−3410.

(30) Lkowicz, J. R. *Principles of Fluorescence Spectroscopy*; Springer: Berlin-Heidelberg, 2006.

(31) van Vugt, L. K.; Piccione, B.; Agarwal, R. Incorporating polaritonic effects in semiconductor nanowire waveguide dispersion. *Appl. Phys. Lett.* **2010**, *97*, 061115.

(32) Holmes, R.; Forrest, S. Strong exciton-photon coupling and exciton hybridization in a thermally evaporated polycrystalline film of an organic small molecule. *Phys. Rev. Lett.* **2004**, *93*, 186404.
(33) Liang, W. Y. Excitons. *Phys. Educ.* **1970**, *5*, 226.
(34) Frenkel, J. On the transformation of light into heat in solids. I. *Phys. Rev.* **1931**, *37*, 17.
(35) Gargas, D. J.; Moore, M. C.; Ni, A.; Chang, S.-W.; Zhang, Z. Y.; Chuang, S. L.; Yang, P. D. Whispering gallery mode lasing from zinc oxide hexagonal nanodisks. *ACS Nano* **2010**, *4*, 3270.